The role of localised compressional Ultra-Low Frequency waves in energetic electron precipitation

I. Jonathan Rae,[1] Kyle R. Murphy,[2] Clare E. J. Watt,[3] Alexa J. Halford,[4] Ian R. Mann,[5] Louis G. Ozeke,[5] David G. Sibeck,[2] Mark A. Clilverd,[6] Craig J. Rodger,[7] Alex. W. Degeling,[8] Colin Forsyth,[1] and Howard J. Singer,[9]

[1]Department of Space and Climate Physics, Mullard Space Science Laboratory, University College London, Holmbury St. Mary, Dorking, Surrey, RH5 6NT, UK.

[2]NASA Goddard Space Flight Centre, Code 674, Greenbelt Maryland, USA

[3]Department of Meteorology, University of Reading, Earley Gate, PO Box 243, Reading RG6 6BB, UK

[4]Department of Physics and Astronomy, Dartmouth College, Hanover, New Hampshire, USA

[5]Department of Physics, University of Alberta, Edmonton, Alberta, Canada. T6G 2G7

[6]British Antarctic Survey (NERC), Cambridge, United Kingdom

[7]Department of Physics, University of Otago, Dunedin, New Zealand

[8]Shandong University, Weihai, Shandong, China

[9]Space Weather Prediction Center, NOAA, Boulder, Colorado, United States

Abstract

Typically, Ultra-Low Frequency (ULF) waves have historically been invoked for radial diffusive transport leading to acceleration and loss of outer radiation belt electrons. At higher frequencies, Very-Low Frequency (VLF) waves are generally thought to provide a mechanism for localized acceleration and loss through precipitation into the ionosphere of radiation belt electrons. In this study we present a new mechanism for electron loss through precipitation into the ionosphere due to a direct modulation of the loss cone via localized compressional ULF waves. We present a case study of compressional wave activity in tandem with riometer and balloon-borne electron precipitation across keV-MeV energies to demonstrate that the experimental measurements can be explained by our new enhanced loss cone mechanism. Observational evidence is presented demonstrating that modulation of the equatorial loss cone can occur via localized compressional wave activity, which greatly exceeds the change in pitch angle through conservation of the first and second adiabatic invariants. The precipitation response can be a complex interplay between electron energy, the localisation of the waves, the shape of the phase space density profile at low pitch angles, ionospheric decay timescales, and the time-dependence of the electron source; we show that two pivotal components not usually considered are localized ULF wave fields and ionospheric decay timescales. We conclude that enhanced precipitation driven by compressional ULF wave modulation of the loss cone is a viable candidate for direct precipitation of radiation belt electrons without any additional requirement for gyroresonant wave-particle interaction. Additional mechanisms would be complementary and additive in providing means to precipitate electrons from the radiation belts during storm-times.

1   Introduction

Energetic electron losses are a critical component of electron dynamics in the inner magnetosphere and outer radiation belt. Although electron dynamics in this region are only partially understood, electron losses can essentially occur either when their drift trajectories intersect with the magnetopause, termed magnetopause shadowing (e.g., West et al., 1972; Turner et al., 2012; Ozeke et al., 2014), or when their bounce trajectories lead them to be lost to the upper atmosphere (e.g. Millan et al., 2002). Traditionally, wave-particle interaction and in particular gyroresonant interaction with plasmaspheric hiss (e.g., Meredith et al., 2007) or whistler-mode waves are invoked as being responsible for pitch-angle scattering of electrons into the loss cone and enhanced precipitation (e.g., Kennel and Petschek, 1966; Millan and Thorne, 2007; Clilverd et al., 2015). Indeed, whistler-mode chorus waves are thought to provide the source of the lower-energy diffuse aurora (e.g., Thorne et al., 2010), and observations of whistler-mode chorus have been shown to be clearly linked to modulation of the diffuse aurora (e.g., Nishimura et al., 2012). However, large whistler-mode chorus amplitudes are waves typically limited to the nighttime and morning sectors of the magnetosphere (Li et al., 2010, Meredith et al., 2012), whereas diffuse auroral processes occur at all magnetic local times (MLTs). More recently, other gyroresonant interactions have also been identified as being a major loss mechanism for relativistic electrons (Breneman et al., 2015), first invoked by Thorne and Kennel (1971). Electromagnetic Ion Cyclotron (EMIC) wave-driven electron loss is now considered to also be a significant contributor to radiation belt losses (e.g., Rodger et al., 2015; Zhang et al., 2016; Hendry et al., 2016, 2017). The source of auroral particle precipitation across all MLT sectors remains to be determined.

Ultra-Low Frequency (ULF) waves have been proposed to provide both resonant (e.g., Elkington et al., 1999; Mann et al., 2013) and diffusive (e.g., Schulz and Lanzerotti, 1974; Brautigam and Albert, 2000) acceleration and transport of electrons. ULF wave precipitation signatures have been observed since the early 1960s (e.g., Ziauddin, 1960; Anger et al., 1963; Brown, 1964), and have been observed in riometer (e.g., Heacock and Hunsucker, 1977; Olson et al., 1980; Spanswick et al., 2005; Beharrel et al., 2010), auroral (e.g., Rae et al., 2007a; Roldugin and Roldugin, 2008) and X-ray related precipitation (e.g., Brito et al., 2012; Motoba et al., 2013; Halford et al., 2015). However, although ULF wave signatures have been observed in precipitation across a wide range of energies from keV to MeV, these waves have only been proposed to be indirectly involved in energetic electron losses. This low-frequency ULF modulation of precipitation in the Pc4-5 frequency range [e.g., Jacobs et al., 1963] is often discussed in terms of the ULF modulation of other wave modes, principally ULF modulation of whistler-mode wave growth rates (Millan et al., 2007; Spanswick et al., 2007; Rae et al., 2007a; Watt et al., 2011; Li et al, 2011; Nishimura et al., 2013; Breneman et al., 2015). In these circumstances, ULF modulation of VLF wave intensities would provide an energy-dependent response where those electrons that are able to resonate with specific VLF wave frequencies would be precipitated. However, the remaining part of the phase space density (PSD) would most likely be unchanged, at least over ULF wave periods (~minutes) where pitch-angle diffusion timescales are usually very long (hours to days – e.g. Horne et al., 2005). Hence, any broadband precipitation must also be explained in full, again at all local times. Recently, Brito et al. [2012; 2015] proposed a new mechanism whereby global ULF waves could be directly implicated in radiation belt losses. The radial motion of relativistic electrons within global-scale compressional ULF waves would mean that electrons would experience larger magnetic fields and shorter field line lengths during the inward motion phase, where conservation of the first and second adiabatic invariants would lead to a gain of parallel energy, altering pitch angles of some electrons sufficiently such that they move into the local loss cone. Although not discussed explicitly by Brito et al., [2012; 2015], this mechanism may work over a large range of electron energies.

In this paper, we explore a related but new mechanism of electron precipitation directly driven by highly-localized compressional ULF waves simply by modulating the equatorial loss cone appreciably from its average, or typical, value. We apply this mechanism initially at geosynchronous (GEO) orbit and find that the average geosynchronous loss cone can increase by up to 50% during large-amplitude compressional ULF waves. Depending upon the shape of the PSD close to the loss cone, this mechanism can provide a significant additional amount of precipitating flux without the requirement for any wave-particle interaction processes. We show clear experimental evidence of ULF wave-modulated precipitating electron fluxes across a wide range of energies (20-400 keV) and conclude that compressional ULF waves should be considered a direct, rather than an indirect, candidate precipitation mechanism for radiation belt electrons, or indeed all electrons close to the loss cone with bounce periods less than the wave period. This mechanism has the potential to directly drive electron precipitation across the entire outer radiation belt and over a wide range of energies, and is not limited to geostationary magnetic latitudes where our observations are concentrated.

2   Instrumentation

In this paper, we primarily utilise data from the GOES fluxgate magnetometers at 0.512s cadence (Singer et al., 1996). However, we also augment this with ground magnetometer data from the CARISMA (Canadian Array for Realtime Investigations of Magnetic Activity; Mann et al., 2008), together with NORSTAR riometer data (http://aurora.phys.ucalgary.ca/norstar/rio/), both at 1s cadence. We further utilize southern hemispheric measurements of bremsstrahlung X-rays, related to the precipitation of energetic electrons from the Balloon Array for Radiation belt Relativistic Electron Loss (BARREL; Millan et al., 2013) Campaign 1, Payload 1H (1H) at both 50 ms resolution (fast X-ray spectrum channel 1 at <180keV X-ray energy) and 32 s cadence (slow X-ray spectrum, for ~30keV-10 MeV X-ray energies).

3   Motivation: 26th January 2013 Case study

Figure 2 shows an overview of in-situ and ground-based observations for a case study of ULF-modulated precipitation during the first NASA BARREL campaign on 26th January 2013. BARREL 1H is in the southern hemisphere immediately conjugate to the NORSTAR ISLL riometer, determined using the T96 magnetic field model. At the period of interest, 1930-2130 UT, GOES-13 is at slightly higher latitudes and around 1 hour of magnetic local time (MLT) to the East.

From top to bottom, Figure 2 shows (a) the GOES-13 and conjugate ground magnetometer magnetic field magnitudes, with (b) the modulation of the loss cone using measured and modeled ionospheric magnetic fields (to be discussed later). Figure 2(c) shows channel 1 from the BARREL fast spectra of <180 keV X-rays and (d) BARREL 1H slow spectra from 50-300keV X-rays. Figure 2 (e) shows riometer absorption from ISLL. Figure 2(f) shows the normalized frequency content of each of these datasets calculated within the vertical lines using FFT analysis of the respective time series from GOES-13 (black), BARREL fast- (blue) and slow- (green and yellow) spectra and the ISLL riometer (red).

Figure 2(a) shows that large-amplitude (25nT peak-to-valley on a background ~85nT) compressional ULF waves are observed at geosynchronous orbit between 4-5mHz (Figure 2a and f) in a temporally localized period between ~1950-2030 UT. Around 20-25 minutes later in UT (2015-2050 UT) and in the southern hemisphere, BARREL 1H measures a clear and large-amplitude ULF-modulated electron precipitation event (Figure 2c,d,f), as does the ISLL riometer, which is conjugate in the northern hemisphere (Figure 2e,f).   Fourier analysis of these time series for the respective periods of modulation (denoted by the dashed vertical black lines) reveals that GOES magnetic field and

BARREL 1H precipitation signatures share a dominant common frequency of 4-5 mHz, and the ISLL riometer a slightly lower dominant frequency of 3-4mHz. Hence, there are common frequencies observed in both geosynchronous magnetometer data and modulated precipitation in the ionosphere. In section 4 we discuss the relevance of the slightly lower frequency observed in the precipitation seen through riometer absorption changes. We note that the precipitation signatures actually correlate best with the compressional ULF wave signature if shifted by 0:30 UT, which suggests that there is in fact a localized source of ULF wave activity drifting slowly westwards or sunwards, e.g., ULF waves driven via an internal source such as unstable ion distributions drifting through that region (Yeoman and Wright, 2001). Further observations from the GOES-15 magnetometer, and MCMU riometer stations (not shown), both located further west from the GOES-13, ISLL and BARREL-1H measurements also indicate that the ULF wave activity is localized in space, and persists for at least 2 hours of Universal Time.

We calculate the linear correlation coefficients for the period of ULF wave activity, noting that there is a large background perturbation to both the ISLL and BARREL data, and that a slightly lower frequency is observed at ISLL for reasons we discuss in the Section 7, but which are primarily due to an ionospheric decay effect. Peak correlation coefficients between GOES and ISLL are 0.5, and between GOES and BARREL is 0.57. Correlation between both ionospheric measurements is significantly better given that both are ionospheric measurements and hence are subject to the same ionospheric decay, peaking at 0.87 between ISLL and BARREL slow spectra at 53keV).

In summary, this case study exhibits localized compressional ULF wave observations from GOES at ~20UT and ~1430 MLT in addition to localized ULF wave-modulated precipitation at ISLL and BARREL 1H at ~2015 UT at ~1315 MLT. Given that the ULF wave signatures are at the same frequency, our hypothesis is that a localized ULF wave field drives ULF-modulated precipitation. The changes in MLT of the localized ULF wave activity as time progresses indicate that these ULF wave signatures must be slowly moving westward, in keeping with an ion-generated compressional ULF wave.

4   What processes could drive localized ULF-modulated precipitation?

Given that the ULF signatures are observed in the same local time region, but are temporally limited in extent, we interpret these combined measurements as clear evidence of a large-amplitude, spatially localized ULF wave field in a highly limited spatial range in the post-noon sector (14-15 MLT). We discuss the potential source of these waves in section 7, but conclude that whatever mechanism leads to the ULF-modulated precipitation event is highly localized in space, and not in time. The question then becomes, what drives this ULF-modulated precipitation?

Whistler-mode waves are invoked to drive precipitation across a wide range of energies (e.g. Miyoshi et al., 2015). In the case of ULF-modulated precipitation, whistler-mode waves are assumed to already exist, and the ULF waves modulate the growth rates of the waves due to a pre-existing source of free energy (e.g., Coroniti and Kennel, 1970). Alternately the VLF spectral distribution is modified via wave-wave interaction between ULF and VLF waves (e.g., Chen, 1974) leading to a ULF-modulated precipitation signature being observed. However, Figure 2 demonstrates that precipitation is not observed by BARREL or ISLL riometer outside of the bounds of the ULF event above the background level, implying that whatever processes cause the precipitation only exist inside the region of ULF waves, indicated in this figure by vertical dashed lines. If whistler-mode waves are present outside of this spatial window, then one would certainly expect to observe unstructured, or differently structured, precipitation to be occurring when the ULF wave field is not present.

In this case study, we show that large-amplitude ULF wave fields are localized to only a fraction of the drift trajectory of an electron, meaning that an energetic electron will encounter a rapid step-change in local magnetic field as it undertakes gradient-curvature drift. If the timescale of this wave is shorter than the drift period, the third adiabatic invariant is likely to be violated. We explore the effects of localized perturbations in magnetic field on the conservation or otherwise of all invariants.

The equatorial bounce loss cone (BLC) characterizes the maximum pitch angle of particles that would precipitate into the ionosphere within one bounce period and is defined as

$$\sin^2\alpha_G = {B_G}/{B_I}$$

(1)

where α_G is the equatorial bounce loss cone angle, B_G is the magnetic field strength in the equatorial plane. The value of B_G is approximated by the magnetic field magnitude at GOES situated close to the equatorial plane, and B_I is the magnetic field strength at the particle mirror point close to the ionosphere. Throughout this paper, we assume that the variation in magnetic field strength observed by GOES can be interpreted as the temporal variation of minimum magnetic field strength along the field line that threads its location. The values of magnetic field in this definition should be understood to be averages over timescales greater than the electron bounce time, which is short compared to a ULF wave period. To estimate the time evolution of equatorial BLC using the observed equatorial magnetic field at GOES for B_G, we must first estimate the magnetic field strength at the ionosphere B_I. Note that of the two magnetic field strengths required for equation (2), $B_G \ll B_I$. It is likely that both B_G and B_I vary as a result of the ULF wave, but the variations in B_G are a significant fraction of B_G whereas the variations in B_I are very small compared to the magnitude of B_I. Therefore the average B_I in the vicinity of the field-line footpoint mapped from the GOES spacecraft could be used in equation (2) with very little loss in accuracy. In this case study, we have compared two estimates for B_I: the projected IGRF field at 100km of the location of the magnetic field footpoint of the GOES position, as mapped using the Tsyganenko T89 [Tsyganenko, 1989] magnetic field model, and the magnetic field strength measured at the SNKQ ground-based magnetometer (being the magnetometer closest to the footprint of GOES West). Figure 2(b) shows the estimated modulation of α_G when using the IGRF field (black) and the measured field at SNKQ (blue). Regardless of the source of the estimated ionospheric field, there is little difference to the modulation of the loss cone, it is only the average size of the loss cone that is different. Since we are interested in the modulation of the loss cone, we will for simplicity use the IGRF field at the location of the GOES footprint to determine B_I in the subsequent analysis, noting that this simplification of dipolar L-shell determination of the first and second adiabatic invariants illustrates the utility of this calculation for enhanced modulation of precipitation, and which becomes increasingly appropriate for locations inside geosynchronous orbits and closer to the radiation belt region.

We now consider how the ULF wave alone could affect the pitch angle of individual particles. Since ULF wave timescales are of order minutes, we can assume that the first and second adiabatic invariants are conserved, but the third is not. Previous studies have investigated how conserving the first and second invariants affects the change in pitch angle and loss cone, under the assumption of a relatively dipolar magnetic field (e.g., Li et al., 1993; Wygant et al., 1994; Halford et al. 2015; Foster et al., 2015). For example, Halford et al. [2015] showed that the change in the equatorial pitch angle of a particle in a slowly-changing and dipolar magnetic field configuration was independent of mass or energy and could be written as:

$$\sin\alpha_{eqf} = -\frac{L_f^{1/2}\cos^2\alpha_{eq0}}{2L_0^{1/2}\sin\alpha_{eq0}} + \frac{1}{2}\left(\frac{L_f\cos^4\alpha_{eq0}}{2L_0\sin^2\alpha_{eq0}} + 4\right)^{1/2}$$

(2)

where α_{eq0} and α_{eqf} are the initial and final equatorial pitch angles, and L_0 and L_f are the initial and final L values of the particle in dipolar L. This equation is valid for the action of a sufficiently low-frequency ULF wave. We use this idealised equation to make a comparison between the changes in particle pitch-angle due to a slowly-changing magnetic field, and the changes in loss-cone due to the same slowly-changing magnetic field. We note here that at the location of GOES, a dipolar approximation is a simplification of the real measured magnetic field. However, as can be seen from Figure 2 and Supplementary Material Figure 1, this is a reasonable assumption given that the measured magnetic field magnitude is ~100nT during the event at geosynchronous orbit.

Figure 3 shows how the equatorial pitch angles $\alpha_{eq,f}$ vary in a ULF wave-modulated magnetic field according to equation (1), where both the first and second adiabatic invariants are conserved. These changes (solid lines) are shown relative to the changes in the BLC α_G according to equation (2) (dashed lines). Figure 3(a) shows a range of low particle pitch-angles (colored lines). The expected change in the BLC is a dashed line, and pitch-angles that fall within the BLC are shaded in grey. For a slowly-varying magnetic field, the change in BLC is far greater than any change in particle pitch angle conserving the 1st and 2nd invariants.

Figure 3(b) shows selected "important" pitch-angles for the case study shown in Figure 2. If only the average magnetic field is considered, the vertical location where the blue (upper) solid line crosses the dashed line would indicate the largest particle pitch-angle to be lost into the BLC. The vertical location where the green (lower) solid line crosses the dashed line indicates the largest pitch-angle that would be lost under the action of the ULF wave, which in this case has an amplitude of 13nT. We will discuss in Section 5 how even these small changes in equatorial loss cone can lead to large changes in precipitating flux.

Figure 3(c) shows the fractional change in $\alpha_{eq,f}$ (solid lines) and α_G (dashed line) to demonstrate that the changes in the BLC are indeed much larger than the changes in the particle equatorial pitch angles and that, for larger ULF wave fields, this effect becomes increasingly pronounced.

5   Implications for Precipitating Electron Flux

The previous section showed that compressional ULF waves can significantly modify the size of the equatorial BLC. In this section, we discuss the implications for driving or enhancing electron precipitation across all energies, likely impacting radiation belt electron dynamics.

Figure 4 illustrates the concept of localised ULF wave driven precipitation, and how this precipitation mechanism is affected by the localisation of the wave and shape of the equatorial distribution in pitch-angle. Figure 4(a) shows a schematic demonstrating how drifting electrons might interact with localized compressional ULF waves and result in electron precipitation, with the Sun to the right of the figure. Electrons undergoing gradient curvature drift around the Earth will encounter a localized region of compressional ULF wave activity, such that electrons that were previously just outside of the bounce (and potentially drift) loss cones and hence were trapped, then find themselves within the loss cone. We reiterate that this is a consequence of conservation of the first and second invariants and the violation of the third adiabatic invariant due to the spatially-localised nature of the ULF waves.

If there are no additional electron sources to replenish those electrons that have been precipitated, and the region of ULF wave activity persists over time scales longer than a drift period, a range of resultant effects may be experienced, from a large precipitation spike into the atmosphere to a longer-lived ULF modulated precipitation signature (see Figure 4(b)). The precipitation signature as detected in the ionosphere depends upon the energy of the electron (i.e. how much time it spends within the ULF wave region) and the phase of its drift orbit relative to the phase and localisation of the ULF oscillation. A single pulse of precipitation would indicate that a compressional ULF wave is acting over a large range of MLT such that electrons across a large fraction of the drift orbit at all energies within the enhanced loss cone would precipitate within the first wave cycle. For more localised compressional wave activity, the ionospheric electron precipitation signature may depend upon (i) the azimuthal wavenumber of the wave, (ii) the phase of the wave as the electron passes through the active region and (iii) the azimuthal extent of the localised wave region. Hence each drift shell up to $\alpha_{G,max}$ will not necessarily be fully depleted after a single drift period. For localised ULF wave activity, the ULF modulated precipitation signature would be maintained as long as the ULF wave was maintained, and until the flux in each drift shell is fully depleted.

The expected precipitation signatures also depends upon whether electrons with pitch angles close to the edge of either the typical or enhanced BLC are replenished from elsewhere in the magnetosphere, i.e., there are additional processes providing a source of electrons on particular drift shells (e.g. the source/seed populations discussed in Jaynes et al., 2015). Substorm injections (e.g., Reeves et al., 1990) and enhanced convection (e.g., Walach and Milan, 2015) can be responsible for the refilling of drift-shells. Electron flux can also be replenished through local wave-particle interaction processes (e.g., Summers and Thorne, 2003).

Note that precipitation as measured in the ionosphere by a riometer or any other instrument which senses atmospheric ionisation changes will not necessarily depend upon time in the same manner as the precipitating flux. The ionospheric recovery times for the conductivity changes must also be taken into account (Clilverd et al., 2007; Rodger et al., 2007). In this instance, each periodic enhancement in the precipitation flux magnitude would have an associated ionospheric decay time, such that additional pulses of precipitation would add to the previous ionospheric enhancement. ULF modulation in the riometer signal would therefore appear as only a small perturbation on a background enhancement as shown in Figure 4 (b). In addition, a long ionospheric decay time relative to the period of wave would result in the ULF modulation of the riometer signal having a slightly lower frequency response than the original ULF wave. We propose this simple explanation for the results shown in Figure 2: a 4-5 mHz precipitation signature is observed by BARREL, but a slightly lower frequency signature is observed in the precipitation as measured by a ground-based riometer.

Naively, for an isotropic distribution, one might expect a given percentage increase in α_G might result in a similar percentage increase in the amount of precipitating flux. However, magnetospheric electron distributions are not generally isotropic with respect to pitch angle, particularly close to the loss cone (e.g., Gu et al., 2011). Typically, electron flux at a constant energy varies as $f = f_0 \sin^n \alpha$ where n can take a range of values e.g. n=0, 0.1, 0.25, 0.5, 1,2,3... and f_0 indicates the value of the flux at 90°. For example, $n = 0$ would correspond to the naïve isotropic assumption discussed above. However, Figure 4 (c) shows how the pitch angle variations due to compressional ULF waves can drive increased precipitation for increasing values of n, using the compressional wave example shown in Figure 1, where α_G = 2.8° and $\alpha_{G,\,max}$ = 3.3°. From Figure 4(c), it can be seen that varying the shape of the pitch angle distribution close to the loss cone can drive significantly more precipitation loss than that implied by the given percentage increase in α_G. For a close to isotropic distribution

i.e., for *n* values between n=0 and n=0.5, an 18% increase in α_G would render a similar ~18% increase in precipitation. However, if the shape of the PSD is closer to the n=3 example, an 18% increase in α_G would render significantly larger percentage increase in precipitating flux, closer to a 100% increase.

6   Statistical Results of GOES Bounce Loss Cone Variations

We employ fourteen years of geosynchronous Geostationary Operational Environmental Satellite (GOES) magnetometer measurements at 1 minute cadence (Singer et al., 1996) to statistically study the variation in the BLC during compressional ULF wave events. Since the GOES satellites are in the geographic equatorial plane, we limit our statistical analysis to satellites located at the GOES West location, since these satellites are closer to the magnetic equator than their GOES East counterparts. As in the previous section, we calculate the variation in BLC using equation (2). The equatorial magnetic field strength B_G is obtained from the GOES measurements, and the ionospheric magnetic field strength B_I is estimated from the IGRF. In order to compile a large database of compressional wave events, we use a 14 year (1995-2008 years) database of GOES data (Ozeke et al., 2012). We limit our analysis to the dayside magnetosphere (06-18 MLT) to concentrate specifically on ULF wave activity and avoid the large-scale topological changes associated with magnetospheric substorms that occur on timescales in the ULF wave band. However, we note that, in principle, our analysis is also relevant to any significant and localized geomagnetic field magnitude variation (as discussed in Section 7).

We define a localized compressional ULF wave event as a quasi-periodic modulation in the magnetic field magnitude above a given amplitude threshold during a one hour analysis window. We calculate the wave amplitude from the power spectral density at each frequency and identify discrete peaks above a 2 nT threshold using a peak finding algorithm. The 2 nT threshold minimizes the chance of the detection of any sudden impulses, or small ULF wave packets, using the same approach adopted in Watt et al. [2011]. Any one hour window with a discrete peak is flagged as an event containing a compressional ULF wave. In order to avoid overlapping windows or double counting, if the hour analyzed contains a compressional ULF wave that fits this criteria within it, this one hour analysis window is shifted by an hour. If the hour analyzed does not contain a compressional ULF wave, the analysis window is stepped by 15 minutes in order to identify the highest number of unique ULF wave events possible. Finally, any hour for which the GOES-measured magnetic field contained a geosynchronous B_{ZGSM} < 30nT were considered to be potentially affected by magnetopause encounters and were thus discarded [c.f. Watt et al., 2011]. In total, through this approach we find 3591 compressional wave events that satisfy our criteria over this 14 year period.

For each of the 3591 identified events, we determine the median and maximum magnetic field magnitude from the GOES 60-minute observations, as well as the median and maximum BLC angle $\alpha_{G,MAX}$ during the hour. In order to determine the relationship between the equatorial loss cone variations with compressional ULF wave activity, we express the percentage change in the BLC (i.e., the maximum change in BLC as a fraction of the median BLC angle) during an hour as a function of compressional wave amplitudes normalized to the background magnetic field magnitude (dB/B_0). Note that the maximum magnetic field strength observed at GOES is equivalent to $B_G=B_0+dB$ and so dB/B_0 is a direct measure of the ULF wave amplitude, but not a direct measure of the change in the loss cone.

Figure 5(a) shows the ULF wave amplitudes as a function of background field strength and their corresponding change in α_G, on a log-log scale. There is a strong linear relationship between α_G and dB/$B_{0,}$ demonstrating that the changes in α_G are indeed linearly related to the fractional change in

the magnetic field magnitudes from localized compressional wave activity. Figure 5(b) reinforces this relationship by displaying a two-dimensional histogram of these points. Finally, Figure 5(c) shows a probability distribution function (PDF) of these events as a function of dB/B_0, where each (vertical)
355 column sums to 100%. Figure 5 (c) shows that there is a strong linear correlation between the size of the compressional wave activity and a most likely given change in the equatorial loss cone. From Figure 5 it can be seen that in the 14 year period studied there are certainly events whereby a narrow-band ULF fluctuation occurs that is of order the background magnetic field strength, and which would correspond to around 50% increase in the size of the ambient BLC. Although fluxes are
360 small at these small pitch angles relative to the core radiation belt population which have pitch angles closer to 90 degrees, we discuss how a direct ULF modulation of the BLC can provide additional precipitation.

7   Discussion

Traditionally, ULF waves are not considered a direct precipitation mechanism for energetic
365 electrons, and instead the ULF modulation of VLF growth rates is invoked to explain precipitation modulated at ULF frequencies [Coroniti and Kennell, 1970]. This is despite clear observational links between ULF magnetic field oscillations and a variety of auroral [Rae et al., 2014], riometer [Spanswick et al., 2005] and bremsstrahlung-related [Brenneman et al., 2015; Halford et al., 2015] electron precipitation signatures. A primary reason for this is that, essentially, global-scale ULF wave
370 fields vary much more slowly than electron bounce times, and therefore cannot force bouncing electrons to violate their 2nd adiabatic invariant (e.g., Olson, 1980). However, in the case where localised ULF wave fields exist only for a fraction of an electron's drift orbit, it is likely that drifting electrons would rapidly encounter magnetic fields that are not varying smoothly or slowly enough to satisfy conservation of the third adiabatic invariant.

375 Previous work has focussed upon resonant global ULF wave processes such as Field Line Resonance driven auroral particle precipitation [e.g., Samson et al., 1991; 1996; 2003; Xu et al., 1993; Milan et al., 2001; Rankin et al., 2005, 2007; Rae et al., 2007a, 2014], as opposed to any direct modulation of the conditions for particle precipitation by the ULF wave itself. Under these circumstances, it is largely electrons with energies less than a few keV that are involved in the FLR-electron interaction.
380 FLRs have been shown to be linked to periodic auroral arc structuring [e.g., Samson et al., 1991; 1994, 1996; Rae et al., 2007a], are capable of modulating existing auroral arcs [e.g., Lotko et al., 1998], or directly powering auroral displays via parallel electric fields accelerating auroral energy electrons [e.g., Rankin et al., 2005, 2007]. More complex auroral structuring can also be explained as a result of two harmonically related FLRs that result of field-aligned current element "braiding"
385 [Milan et al., 2001]. However, it is unlikely that electrons above ~keV energies could be accelerated in the field-aligned direction in any of these scenarios, as toroidal mode FLRs have no compressional component, although they have recently been postulated to play a secondary role [e.g., Motoba et al., 2015].

At electron energies above ~keV, a plethora of observations exist that link ULF waves in ground
390 magnetometer and riometer absorption [e.g., Ziauddin, 1960; Anger et al., 1963; Brown, 1964; Parthasarathy and Hessler, 1964; Hargreaves, 1969; Yuan and Jacka, 1969; Hunsucker et al., 1972; Berkey, 1974; Brown, 1975; Heacock and Hunsucker, 1977; Olson et al., 1980; Paquette et al., 1994; Posch et al., 1999; Spanswick et al., 2005; Rae et al., 2007a; Roldugin and Roldugin, 2008; Beharrell et al., 2010]. Spanswick et al. [2005] used statistics of NORSTAR riometer measurements to
395 investigate the relationship between Pc5 wave power observed in riometer data and FLRs observed in ground magnetometer data, finding that when significant ULF wave power was observed in riometer absorption, there was always generally a corresponding Pc5 wave signature in ground

magnetometer data. In addition, it was found that FLR Pc5 activity was more efficient at producing the riometer modulation than non-FLR Pc5 activity. Spanswick et al. [2005] concluded that the most likely scenario was that when a suitable energetic electron population in the inner magnetosphere was present, resonant ULF waves could play a role in their precipitation but that pitch-angle scattering from some other plasma wave (for example whistler-mode waves) was required as well before both ground magnetometer and riometer would observe a ULF modulated signal. From a theoretical perspective (Coroniti and Kennel, 1970, Watt et al., 2011), a variation in magnetic field strength (i.e. a compressional component of the wave magnetic field) is required to modulate VLF growth rates. Moreover, a variation in magnetic field strength that is in direct antiphase with the cold plasma number density (c.f. Li et al., [2011] and Watt et al., [2011]) is required to modify VLF growth rates sufficiently to account for the changes in precipitation.   Since FLRs are where energy from a propagating compressional wave couples to the shear mode (Samson et al., 1992), it is not clear whether the wave properties necessary to modify VLF wave growth rates are satisfied in an FLR. We postulate in this study that the reason is that the compressional component of the FLR driver may be the direct generator of ULF-modulated riometer absorption, rather than the action of the FLR itself. Specific case studies of a simultaneous compressional ULF wave and an FLR have been presented in the literature (e.g., Rae et al., 2007a). The evidence presented here suggests that an alternative explanation for the modulation of ULF-precipitation in this and other cases is the direct modulation of the equatorial BLC by the compressional component of the ULF wave.

Direct enhancement of the local equatorial bounce loss cone enhances other mechanisms for precipitation of electrons from the magnetosphere. Brito et al. [2012; 2015] used MHD simulations to show that the radial displacement of electrons due to global-scale compressional ULF waves can itself lead to enhanced precipitation. The radial motion of the electrons encountering a compressional ULF wave causes their trajectories to move closer to the Earth into a stronger magnetic field, where the loss cone is larger. Additionally, the inward radial motion of the electrons leads them into regions with shorter field lines, where they gain perpendicular energy due to conservation of the first adiabatic invariant and parallel energy due to conservation of the second adiabatic invariant. In this paper we show additional precipitation effects if these ULF wave fields are localized; under these circumstances, the loss-cone is locally and abruptly modified as a function of time through the action of the compressional ULF waves themselves. Compressional magnetospheric ULF waves at geosynchronous orbit can have sufficient amplitudes to locally enhance the size of the bounce loss-cone by over 50%. Of course, this effect (shown in Figure 4) depends upon the ratio of the wave amplitude to the background magnetic field, and the background magnetic field varies as a function of radial distance r as roughly r^{-3}. Our observations are confined to geosynchronous orbit, to which the majority of riometer absorption modulation also map (Spanswick et al., 2005). However, closer to the heart of the Outer Radiation Belts at $L=4-5$, where the field strength increases and ULF modulated precipitation is often seen (e.g., Brenneman et al., 2015; Brito et al., 2015), the fractional enhancement in the traditional loss cone will become smaller for a given ULF wave amplitude. However, again there are competing effects to be considered, given that equatorial BLC also increases with decreasing radial distance, this means that both the equatorial loss cone and compressional ULF wave amplitudes must be computed across all radial distances in order to determine their effect across the entire outer Radiation Belt region.

The direct enhancement of the BLC by a localised compressional ULF wave will also greatly enhance any precipitation mechanism that is due to pitch-angle scattering. Whistler-mode chorus (see Millan and Thorne, 2007 for a comprehensive review) is often invoked to pitch angle scatter radiation belt electrons outside of the plasmapause, with plasmaspheric hiss acting in a similar way inside of the plasmapause (e.g., Breneman et al., 2015). Electromagnetic Ion Cyclotron (EMIC) waves have also

445   been shown to play a role in enhanced relativistic electron precipitation (e.g., Rodger et al., 2008; Carson et al., 2013; Clilverd et al., 2015) through cyclotron resonant interactions. Pitch-angle scattering rates depend upon the wavenormal angle and power spectral densities of the whistler-mode chorus (e.g, Ni et al., 2011). However pitch-angle diffusion rates for a 30keV electron at geosynchronous orbit range from 10^{-3}-10^{-4} s^{-1}, which is comparable to Pc5 ULF wave frequencies. By

450   contrast, inside the plasmasphere, plasmaspheric hiss can have pitch-angle diffusion rates of 10^{-2}-10^{0} s^{-1} (e.g., Breneman et al., 2015). As EMIC waves are the left-hand counterpart of whistler-mode waves, there would be no reason not to expect that EMIC wave growth would also be affected by large-amplitude monochromatic changes of the magnetic field magnitude and number density either, as Loto'aniu et al. [2009] discussed.

455   Whistler-mode precipitation will be enhanced by a temporally-varying loss-cone for two reasons. First, pitch-angle scattering increases the flux at pitch angles close to the bounce loss cone while our mechanism increases the size of the bounce loss cone thus leading to enhanced loss. Second, by increasing the amount of precipitation, the anisotropy that drives whistler-mode waves unstable may also increase during different phases of the wave leading to either enhanced wave amplitudes

460   or longer lifetime and thus increased precipitation. This explanation provides additional insight into events discussed by Halford et al. [2015] and Breneman et al. [2015], where ULF waves were proposed to be modulating the resonance condition, leading to both an enhanced background level of precipitation and modulation at ULF frequencies. This symbiotic relationship, comparable to that espoused by Baumjohann et al. [2000] regarding whistler-mode waves inside mirror-mode waves in

465   the dawn sector magnetosphere (e.g., Rae et al., 2007b), is ripe for further exploration.

      Most importantly with regards to the results in this paper, it remains to be established whether ULF waves and ULF-modulated precipitation are observed without the presence of whistler-mode chorus (e.g., Nishimura et al. 2013) or plasmaspheric hiss (e.g., Breneman et al., 2015). Our results suggest that such a precipitation mechanism is possible in theory and offers a suggested mechanism for the

470   case study shown in Figure 2, in a region typically associated with limited VLF wave activity and where no enhanced precipitation outside of the compressional ULF wave region is observed. Future work will explore the wealth of ground and space-based observations available in the Van Allen Probe era to identify whether ULF-modulated precipitation can indeed exist without any VLF pitch-angle scattering mechanism.

475   The localisation of the ULF pulsation appears to be very important for the precipitation of electrons. Localised dayside ULF wave fields are often referred to as drift-bounce resonance or "storm-time Pc5 waves" and are thought to be driven by unstable ion distributions emanating from magnetotail injections (e.g., Southwood et al., 1969; Lanzerotti et al., 1969; Wright et al., 2001). They are detected mainly in the afternoon/evening sector of the magnetosphere (e.g., Anderson et al., 1990).

480   Our case study (Figure 1) shows ULF compressional wave activity in the afternoon sector. However, in our statistical study, we show observations of compressional pulsations at geosynchronous orbit across all of the dayside magnetosphere, and so other generation mechanisms may also play a role (e.g., mirror-mode waves in the dawn sector e.g., Zhu and Kivelson, 1994; Vaivads et al., 2001; Rae et al., 2007b; Constantinescu et al., 2009; Liu et al., 2016).   We recognise that mode structure along

485   the field is important for determining changes in BLC at any point along the geomagnetic field due to ULF wave modulation (e.g., Takahashi et al., 1987; Ozeke and Mann, 2004; Perry et al., 2005). Indeed, it is interesting to note that localized compressional waves (e.g., Rae et al., 2007; Liu et al., 2016) would act to trap particles primarily with pitch angles closer to 90 degrees in magnetic bottles via the mirror effect. Hence, trapping of high pitch angle particles may act in concert with the

490   enhanced precipitation of low pitch angle particles. To confirm that our assumptions are correct,

future work will use electric, magnetic and plasma density measurements to characterise mode structure and perform more accurate calculation of the change in the equatorial BLC in each case. Future work will utilise a more realistic three dimensional magnetospheric wave model (Degeling et al., 2010) where localisation of the waves in magnetic local time, and realistic field-aligned structures can be reproduced. By doing this, electrons can then be traced through to see how their behaviour is modified and the loss-cone is modified due to the presence of the localised, compressional ULF waves.

8   Conclusion

This paper explored the potential role of localised compressional ULF waves as a candidate mechanism to directly enhance electron precipitation by simple modulation of the local bounce loss cone. Periodic magnetic compression of a localised magnetospheric region on long period timescales relative to the gyration and bounce allows conservation of the first and second adiabatic invariants but a clear opportunity to violate the third invariant. We demonstrate that the change in pitch angle of a given electron due to the conservation of the first and second invariants (Figure 3) is far smaller than the change in loss cone due to the localised ULF wave (Figure 2 and Figure 4). In this way, we show that localised compressional ULF waves can directly contribute to electron precipitation.

Previous studies (e.g., Brito et al., 2012; 2015) have focussed on the role of global compressional ULF waves in driving radial motion of radiation belt electrons to additionally precipitate. Direct modulation of the loss cone differs from any other mechanism traditionally invoked to explain, in particular, radiation belt electron losses during active times. ULF modulation of the bounce loss cone would be enhanced during active times, such as during a storm main phase where compressional ULF wave amplitudes are largest and up to ~2 orders of magnitude higher than statistically found (Murphy et al., 2015). We note here that this mechanism will also operate across all electron energies, but with subtly different observational characteristics, potentially explaining how low-energy auroral (e.g., Samson et al., 1991), keV (e.g., Spanswick et al., 2005), 100s keV (e.g., Breneman et al., 2015) and MeV (e.g., Foat et al., 1998; Millan et al., 2002, Woodger et al 2015) electron energies can all display ULF modulation, which no one single gyroresonant process can be invoked to explain.

Statistically, we show that large-amplitude highly-localised compressional ULF waves can modulate the loss cone by ±20%, which in turn allows a significantly greater fraction of the electron PSD to precipitate than previously thought. Importantly, this requires no other wave-particle interaction to cause precipitation of energetic electrons with pitch angles outside of the traditional loss cone, although this mechanism would be enhanced by local pitch-angle scattering to refill the near-loss cone population. Hence, what fraction of this distribution is locally precipitated depends upon the strength of the perturbation, local magnetic field magnitude, shape of the pitch angle distribution close to the traditional loss cone and the nature of any additional sources of energetic electrons into the ULF region (e.g., substorm injections) or near the loss cone (e.g., pitch-angle scattering due to whistler-mode waves). Since this mechanism does not require the presence or the absence of VLF wave-particle interaction, we simply point out that localised compressional waves should be considered along with other precipitation mechanisms within the current literature.

We show direct evidence of ULF wave modulated precipitation across the energy ranges measured by riometers and BARREL, which is spatially correlated with localised large-amplitude (~15% of the ambient magnetic field) compressional ULF wave activity in the afternoon sector. Within this case study we show clear evidence that the ULF wave fields are spatially localised, although we note here

that there is no means to investigate other precipitation sources for this case which would be expected from pitch-angle scattering mechanisms such as whistler-mode chorus or plasmaspheric hiss.

540 We believe that this mechanism warrants further study to determine whether compressional waves and ULF modulated losses are indeed causally related and whether such loss can routinely occur independently of gyro-resonant interactions.

Acknowledgements

555

9   References

Anderson, B. J., M. J. Engebretson, S. P. Rounds, L. J. Zanetti, and T. A. Potemra (1990), A statistical study of Pc3-5 pulsations observed by the AMPTE/CCE magnetic field experiment 1, Occurrence distributions, J. Geophys. Res., 95(A7), 10495–10523.

560 Anger, C. D., R. R. Brown, D. S. Evans, and J. R. Barcus (1963), Long period pulsations in electron precipitation associated with hydromagnetic waves in auroral zone, J. Geophys. Res., 68(10), 3306–3310.

Barfield, J. N., R. L. McPherron, P. J. Coleman Jr, and D. J. Southwood (1972), Storm associated Pc5 micropulsation events observed at the synchronous equatorial orbit, J. Geophys. Res., 77(1), 143–
565 158, doi:10.1029/JA077i025p04720.

Beharrell, M., A. J. Kavanagh, and F. Honary (2010), On the origin of high m magnetospheric waves, J. Geophys. Res., 115, A02201, doi:10.1029/2009JA014709.

Brautigam, D., and J. Albert (2000), Radial diffusion analysis of outer radiation belt electrons during the October 9, 1990, magnetic storm, J. Geophys. Res., 105, 291–309, doi:10.1029/1999JA900344.

570 Breneman, A. W., A. Halford, R. Millan, M. McCarthy, J. Fennell, J. Sample, L. Woodger, G. Hospodarsky, J. R. Wygant, C. A. Cattell, J. Goldstein, D. Malaspina and C. A. Kletzing (2015), Nature, 523, 193-195, doi:10.1038/nature14515.

Brito, T., L. Woodger, M. Hudson, and R. Millan (2012), Energetic radiation belt electron precipitation showing ULF modulation, Geophys. Res. Lett., 39, L22104, doi:10.1029/2012GL053790.

575 Brito, T., M. K. Hudson, B. Kress, J. Paral, A. Halford, R. Millan, and M. Usanova (2015), Simulation of ULF wave-modulated radiation belt electron precipitation during the 17 March 2013 storm. J. Geophys. Res. Space Physics, 120, 3444–3461. doi: 10.1002/2014JA020838.

Brown, R. R. (1964), Study of slowly varying and pulsating ionospheric absorption events in auroral zone, J. Geophys. Res., 69(11), 2315–2321.

580 Barfield, J. N., R. L. McPherron, P. J. Coleman Jr, and D. J. Southwood (1972), Storm associated Pc5 micropulsation events observed at the synchronous equatorial orbit, J. Geophys. Res., 77(1), 143–158, doi:10.1029/JA077i025p04720.

Baumjohann, W., E. Georgescu, K.-H. Fornacon, H. U. Auster, R. A. Treumann, G. Haerendel (2000), Magnetospheric lion roars, Ann. Geophys., 18, 4, 406-410.

585 Carson, B. R., C. J. Rodger, and M. A. Clilverd (2013), POES satellite observations of EMIC-wave driven relativistic electron precipitation during 1998–2010, J. Geophys. Res. Space Physics, 118, 232–243, doi:10.1029/2012JA017998

Chen, L. (1974), Theory of ULF modulation of VLF emissions. Geophys. Res. Lett., 1: 73–75. doi:10.1029/GL001i002p00073

590 Clilverd, M. A., C. J. Rodger, R. M. Millan, J. G. Sample, M. Kokorowski, M. P. McCarthy, T. Ulich, T. Raita, A. J. Kavanagh, and E. Spanswick (2007), Energetic particle precipitation into the middle atmosphere triggered by a coronal mass ejection, J. Geophys. Res., 112, A12206, doi:10.1029/2007JA012395.

Clilverd, M. A., R. Duthie, R. Hardman, A. T. Hendry, C. J. Rodger, T. Raita, M. Engebretson, M. R.
595 Lessard, D. Danskin, and D. K. Milling (2015), Electron precipitation from EMIC waves: A case study from 31 May 2013. J. Geophys. Res. Space Physics, 120, 3618–3631. doi: 10.1002/2015JA021090.

Clilverd, M. A., C. J. Rodger, M. Andersson, P. T. Verronen, and A. Seppälä (2015a), Linkages between the radiation belts, polar atmosphere and climate: electron precipitation through wave particle interactions, in Waves, particles and storms in geospace, edited by I. Mann et al., Oxford University
600 Press.

Constantinescu, O. D., et al. (2009), THEMIS observations of duskside compressional Pc5 waves, J. Geophys. Res., 114, A00C25, doi:10.1029/2008JA013519.

Coroniti, F. V., and C. F. Kennel (1970), Electron precipitation pulsations, J. Geophys. Res., 75(7), 1279–1289.

605 Degeling, A. W., R. Rankin, K. Kabin, I. J. Rae, and F. R. Fenrich (2010), Modeling ULF waves in a compressed dipole magnetic field, J. Geophys. Res., 115, A10212, doi:10.1029/2010JA015410.

Elkington, S. R., M. K. Hudson and A. A. Chan (1999), Acceleration of relativistic electrons via drift-resonant interaction with toroidal-mode Pc-5 ULF oscillations, Geophysical Research Letters, 26, 3273-3276.

610 Engebretson, M. J., and L. J. Cahill Jr. (1981), Pc5 pulsations observed during the June 1972 geomagnetic storm, J. Geophys. Res., 86(A7), 5619–5631, doi:10.1029/JA086iA07p05619.

Foat, J.E., Lin, R.P., Smith, D.M., Fenrich, F., Millan, R., Roth, I., Lorentzen, K.R., McCarthy, M.P., Parks, G.K. and Treilhou, J.P. (1998). First detection of a terrestrial MeV X-ray burst. Geophysical Research Letters 25: doi: 10.1029/1998GL900134. issn: 0094-8276.

615   Gu, X., Z. Zhao, B. Ni, Y. Shprits, and C. Zhou (2011), Statistical analysis of pitch angle distribution of radiation belt energetic electrons near the geostationary orbit: CRRES observations, J. Geophys. Res., 116, A01208, doi:10.1029/2010JA016052.

Halford, A. J., S. L. McGregor, K. R. Murphy, R. M. Millan, M. K. Hudson, L. A. Woodger, C. A. Cattel, A. W. Breneman, I. R. Mann, W. S. Kurth, G. B. Hospodarsky, M. Gkioulidou, and J. F. Fennell (2015),
620   BARREL observations of an ICME-shock impact with the magnetosphere and the resultant radiation belt electron loss. J. Geophys. Res. Space Physics, 120, 2557–2570, doi: 10.1002/2014JA020873.

Heacock, R. R., and R. D. Hunsucker (1977), Study of concurrent magnetic- field and particle precipitation pulsations, 0.005 to 0.5 Hz, recorded near College, Alaska, J. Atmos. Terr. Phys., 39(4), 487–501.

625   Hendry, A. T., Rodger, C. J., Clilverd, M. A., Thomson, N. R., Morley, S. K. and Raita, T. (2012) Rapid Radiation Belt Losses Occurring During High-Speed Solar Wind Stream–Driven Storms: Importance of Energetic Electron Precipitation, in Dynamics of the Earth's Radiation Belts and Inner Magnetosphere (eds D. Summers, I. R. Mann, D. N. Baker and M. Schulz), American Geophysical Union, Washington, D. C.. doi: 10.1029/2012GM001299

630   Hendry, A. T., C. J. Rodger, M. A. Clilverd, M. J. Engebretson, I. R. Mann, M. R. Lessard, T. Raita, and D. K. Milling, Confirmation of EMIC wave driven relativistic electron precipitation, J. Geophys. Res., 121, 5366–5383, doi:10.1029/2015JA022224, 2016.

Hendry, A. T., C. J. Rodger, and M. A. Clilverd (2017), Evidence of sub-MeV EMIC-driven electron precipitation, Geophys. Res. Lett., 44, 1210–1218, doi:10.1002/2016GL071807.

635   Horne, R. B., S. A. Glauert, and R. M. Thorne (2003), Resonant diffusion of radiation belt electrons by whistler-mode chorus, Geophys. Res. Lett., 30, 1493, doi:10.1029/2003GL016963

Horne, R. B., R. M. Thorne, S. A. Glauert, J. M. Albert, N. P. Meredith, and R. R. Anderson (2005), Timescale for radiation belt electron acceleration by whistler mode chorus waves, J. Geophys. Res., 110, A03225, doi:10.1029/2004JA010811.

640   Hutchinson, J. A., D. M. Wright, and S. E. Milan (2011), Geomagnetic storms over the last solar cycle: A superposed epoch analysis, J. Geophys. Res., 116, A09211, doi:10.1029/2011JA016463.

Jaynes, A. N., et al. (2015), Source and seed populations for relativistic electrons: Their roles in radiation belt changes, J. Geophys. Res. Space Physics, 120, 7240–7254, doi:10.1002/2015JA021234.

Kataoka, R., and Y. Miyoshi (2010), Why are relativistic electrons persistently quiet at
645   geosynchronous orbit in 2009? Space Weather, 8, S08002, doi:10.1029/2010SW000571.

Kennel, C. F., and H. E. Petschek (1966), Limit on stably trapped particle fluxes, J. Geophys. Res., 71(1), 1–28, doi:10.1029/JZ071i001p00001.

Kepko, L., and H. E. Spence (2003), Observations of discrete, global magnetospheric oscillations directly driven by solar wind density variations, J. Geophys. Res., 108, 1257,
650   doi:10.1029/2002JA009676, A6.

Kilpua, E. K. J., H. Hietala, D. L. Turner, H. E. J. Koskinen, T. I. Pulkkinen, J. V. Rodriguez, G. D. Reeves, S. G. Claudepierre, H. E. Spence (2015), Unraveling the drivers of the storm time radiation belt response, Geophysical Research Letters, 42, 3076-3084.

Lanzerotti, L. J., A. Hasegawa, and C. G. Maclennan (1969), Drift mirror instability in the magnetosphere: Particle and field oscillations and electron heating, J. Geophys. Res., 74(24), 5565-5578, doi:10.1029/JA074i024p05565.

Li, W., et al. (2010), THEMIS analysis of observed equatorial electron distributions responsible for the chorus excitation, J. Geophys. Res., 115, A00F11, doi:10.1029/2009JA014845.

Li, W., R. M. Thorne, J. Bortnik, Y. Nishimura, and V. Angelopoulos (2011), Modulation of whistler-mode chorus waves: 1. Role of compressional Pc4–5 pulsations, J. Geophys. Res., 116, A06205, doi:10.1029/2010JA016312.

Liu, H., et al. (2016), Compressional ULF wave modulation of energetic particles in the inner magnetosphere, J. Geophys. Res. Space Physics, 121, 6262–6276, doi:10.1002/2016JA022706.

Lotko, W., A. V. Streltsov, and C. W. Carlson (1998), Discrete auroral arc, electrostatic shock and suprathermal electrons powered by dispersive, anomalously resistive field line resonance, Geophys. Res. Lett. 25, p 4449-4452.

Loto'aniu, T. M., Fraser, B. J., and Waters, C. L. (2009),The modulation of electromagnetic ion cyclotron waves by Pc 5 ULF waves, Ann. Geophys., 27, 121-130, doi:10.5194/angeo-27-121-2009.

Mann, I. R., et al. (2013), Discovery of the action of a geophysical synchrotron in the Earth's Can Allen radiation belts, Nature Communications, 4, 2785, doi: 10.1038/ncomms3795.

Meredith, N. P., R. B. Horne, A. Sicard-Piet, D. Boscher, K. H. Yearby, W. Li, and R. M. Thorne (2012), Global model of lower band and upper band chorus from multiple satellite observations, J. Geophys. Res., 117, A10225, doi:10.1029/2012JA017978.

Milan, S., N. Sato, M. Ejiri, and J. Moen (2001), Auroral forms and the field-aligned current structure associated with field line resonances, J. Geophys. Res., 106(A11), 25,825–25,833, doi:10.1029/2001JA900077.

Millan, R. M., R. P. Lin, D. M. Smith, K. R. Lorentzen, and M. P. McCarthy (2002), X-ray observations of MeV electron precipitation with a balloon-borne germanium spectrometer, Geophys. Res. Lett., 29(24), 2194, doi:10.1029/2002GL015922.

Millan, R., and R. Thorne (2007), Review of radiation belt relativistic electron losses, J. Atmos. Sol. Terr. Phys., 69(3), 362–377, doi:10.1016/j.jastp.2006.06.019.

Millan, R. M., et al. (2013), The Balloon Array for RBSP Relativistic Electron Losses (BARREL), Space Sci. Rev., 179(1-4), 503–530, doi:10.1007/s11214-013-9971-z.

Miyoshi, Y., S. Oyama, S. Saito, S. Kurita, H. Fujiwara, R. Kataoka, Y. Ebihara, C. Kletzing, G. Reeves, O. Santolik, M. Clilverd, C. J. Rodger, E. Turunen, and F. Tsuchiya (2015), Energetic electron precipitation associated with pulsating aurora: EISCAT and Van Allen Probe observations. J. Geophys. Res. Space Physics, 120, 2754–2766, doi: 10.1002/2014JA020690.

Moon, G.-H., B.-H. Ahn, Y. Kamide, and G. D. Reeves (2004), Correlation between particle injections observed at geosynchronous orbit and the Dst index during geomagnetic storms, J. Geophys. Res., 109, A10213, doi:10.1029/2004JA010390

Motoba, T., K. Takahashi, J. Gjerloev, S. Ohtani, and D. K. Milling (2013), The role of compressional Pc5 pulsations in modulating precipitation of energetic electrons, J. Geophys. Res. Space Physics, 118, 7728–7739, doi:10.1002/2013JA018912.

Murphy, K. R., I. R. Mann, D. G. Sibeck, On the dependence of storm-time ULF wave power on magnetopause location: Impacts for ULF wave radial diffusion, Geophy. Res. Lett., accepted.

Ni, B., Y. Shprits, M. Hartinger, V. Angelopoulos, X. Gu, and D. Larson (2011), Analysis of radiation belt energetic electron phase space density using THEMIS SST measurements: Cross-satellite calibration and a case study, J. Geophys. Res., 116, A03208, doi:10.1029/2010JA016104.

Nishimura, Y., et al, (2013), Structures of dayside whistler-mode waves deduced from conjugate diffuse aurora, J. Geophys. Res. Space Physics, 118, 664–673, doi:10.1029/2012JA018242.

Olson, J. V., G. Rostoker, and G. Olchowy (1980), A study of concurrent riometer and magnetometer variations in the Pc 4–5 pulsation band, J. Geophys. Res., 85(A4), 1695–1702.

Ozeke, L. G., and I. R. Mann. (2004), Modeling the properties of guided poloidal Alfvén waves with finite asymmetric ionospheric conductivities in a dipole field, Journal of Geophysical Research: Space Physics, 109,A5

Ozeke, L. G., I. R. Mann, and J. T. Mathews (2005), The influence of asymmetric ionospheric Pedersen conductances on the field-aligned phase variation of guided toroidal and guided poloidal Alfvén waves., Journal of Geophysical Research: Space Physics, 110, A8

Ozeke, L. G., Mann, I. R., Murphy, K. R., Rae, I. J., Milling, D. K., Elkington, S. R., … Singer, H. J. (2012). ULF wave derived radiation belt radial diffusion coefficients. Journal of Geophysical Research: Space Physics, 117(4), doi: 10.1029/2011JA017463, 1–16.

Ozeke L.G., Mann I.R., Turner D.L., Murphy K.R., Degeling A.W., Rae I.J., Milling D.K., Modeling cross L shell impacts of magnetopause shadowing and ULF wave radial diffusion in the Van Allen belts, 2014b, Geophysical Research Letters, 41, 6556.

Perry, K. L., M. K. Hudson, and S. R. Elkington (2005), Incorporating spectral characteristics of Pc5 waves into three-dimensional radiation belt modeling and the diffusion of relativistic electrons, J. Geophys. Res., 110, A03215, doi:10.1029/2004JA010760.

Rae, I. J., I. R. Mann, Z. C. Dent, D. K. Milling, E. F. Donovan, and E. Spanswick (2007a), Multiple field line resonances: Optical, magnetic and absorption signatures, Planet. Space Sci., 55, 701-713.

Rae, I. J., I. R. Mann, C. E. J. Watt, L. M. Kistler, and W. Baumjohann (2007b), Equator-S observations of drift mirror mode waves in the dawnside magnetosphere, J. Geophys. Res., 112, A11203, doi:10.1029/2006JA012064.

Rae, I. J., K. R. Murphy, C. E. J. Watt, G. Rostoker, R. Rankin, I. R. Mann, C. R. Hodgson, H. U. Frey, A. W. Degeling, and C. Forsyth (2014), Field line resonances as a trigger and a tracer for substorm onset, J. Geophys. Res. Space Physics, 119, 5343–5363, doi:10.1002/2013JA018889.

Rankin, R., K. Kabin, J. Y. Lu, I. R. Mann, R. Marchand, I. J. Rae, V. T. Tikhonchuk, and E. F. Donovan (2005), Magnetospheric field-line resonances: Ground-based observations and modeling, Journal of Geophysical Research-Space Physics, 110, A10S09.

730   Rankin, R., C. E. J. Watt, and J. C. Samson (2007), Self-consistent wave-particle interactions in dispersive scale long-period field-line-resonances, Geophys. Res. Lett., 34, L23103, doi:10.1029/2007GL031317

Reeves, G. D., T. A. Fritz, T. E. Cayton, and R. D. Belian (1990), Multi-satellite measurements of the substorm injection region, Geophys. Res. Lett.,17(11), 2015–2018, doi:10.1029/GL017i011p02015.

Rodger, C. J., M. A. Clilverd, D. Nunn, P. T. Verronen, J. Bortnik, and E. Turunen (2007), Storm time,
735   short-lived bursts of relativistic electron precipitation detected by subionospheric radio wave propagation, J. Geophys. Res., 112, A07301, doi:10.1029/2007JA012347.

Rodger, C. J., T. Raita, M. A. Clilverd, A. Seppälä, S. Dietrich, N. R. Thomson, and T. Ulich (2008), Observations of relativistic electron precipitation from the radiation belts driven by EMIC waves, Geophys. Res. Lett., 35, L16106, doi:10.1029/2008GL034804.

740   Rodger, C. J., M. A. Clilverd, A. J. Kavanagh, C. E. J. Watt, P. T. Verronen, and T. Raita (2012), Contrasting the responses of three different ground-based instruments to energetic electron precipitation, Radio Sci., 47, RS2021, doi:10.1029/2011RS004971.

Rodger, C. J., A. T. Hendry, M. A. Clilverd, C. A. Kletzing, J. B. Brundell, and G. D. Reeves (2015), High-resolution in situ observations of electron precipitation-causing EMIC waves, Geophys. Res. Lett., 42,
745   9633–9641, doi:10.1002/2015GL066581.

Roldugin, V. C., and A. V. Roldugin (2008), Pc5 pulsations on the ground, in the magnetosphere, and in the electron precipitation: Event of 19 January 2005, J. Geophys. Res., 113, A04222, doi:10.1029/ 2007JA012553.

Samson, J. C., T. J. Hughes, F. Creutzberg, D. D. Wallis, R. A. Greenwald, and J. M. Ruohoniemi (1991),
750   Observations of a detached discrete are in association with field line resonances, J. Geophys. Res., 96, 15,683.

Samson, J. C., B. G. Harrold, J. M. Ruohoniemi, R. A. Greenwald, A. D. M. Walker (1992), Field line resonances associated with MHD waveguides in the magnetosphere, Geophys. Res. Lett., 19, doi:10.1029/92GL00116.

755   Samson, J. C., L. L. Cogger, and Q. Pao (1996), Observations of field line resonances, auroral arcs, and auroral vortex structures, Journal of Geophysical Research-Space Physics, 101, 17373-17383.

Samson, J. C.: Mapping substorm intensifications from the ionosphere to the magnetosphere, in: Proc. Second International Conference on Substorms (ICS-2), edited by: Kan, J. R., Craven, J. D., and Akasofu, S.-I., p. 237, Geophysical Institute, University of Alaska Fairbanks, 1994

760   Samson, J. C., R. Rankin, and V. T. Tikhonchuk (2003), Optical signatures of auroral arcs produced by field line resonances: comparison with satellite observations and modeling, Annales Geophysicae, 21, 933-945.

Schulz, M., and L. J. Lanzerotti (1974), Particle Diffusion in the Radiation Belts, Phys. Chem. Space, vol. 7, 215 pp., Springer, New York.

765   Singer, H. J., L. Matheson, R. Grubb, A. Newman, and S. D. Bouwer (1996), Monitoring space weather with the GOES magnetometers, Proc. SPIE Int. Soc. Opt. Eng., 2812, 299–308.

Southwood, D. J., J. W. Dungey, and R. L. Etherington (1969), Bounce resonant interaction between pulsations and trapped particles, Planet Space Sci., 17, 349

770 Spanswick, E., E. Donovan, and G. Baker (2005), Pc5 modulation of high energy electron precipitation: Particle interaction regions and scattering efficiency, Ann. Geophys., 23(5), 1533–1542.

Summers, D., and R. M. Thorne (2003), Relativistic electron pitch-angle scattering by electromagnetic ion cyclotron waves during geomagnetic storms, J. Geophys. Res., 108, 1143, doi:10.1029/2002JA009489, A4.

775 Takahashi, K., J. F. Fennell, E. Amata, and P. R. Higbie (1987), Field-aligned structure of the storm time Pc5 wave of November 14-15, 1979, J. Geophys. Res., 92(A6), 5857–5864, doi:10.1029/JA092iA06p05857.

Thorne, R. M., and C. F. Kennel (1971), Relativistic electron precipitation during magnetic storm main phase, J. Geophys. Res., 76(19), 4446–4453, doi:10.1029/JA076i019p04446.

780 Thorne, R. M., B. Ni, X. Tao, R. B. Horne, N. P. Meredith (2010), Scattering by chorus waves as the dominant cause of diffuse auroral precipitation, Nature, 467, 943-946.

Thorne, R. M., et al. (2013), Rapid local acceleration of relativistic radiation-belt electrons by magnetospheric chorus, Nature, 504, 411-414.

Turner, D. L., Y. Shprits, M. Hartinger, and V. Angelopoulos (2012), Explaining sudden losses of 785 outer radiation belt electrons during geomagnetic storms, Nat. Phys., 8, 208–212.

Vaivads, A., W. Baumjohann, G. Haerendel, R. Nakamura, H. Kucharek, B. Klecker, M. R. Lessard, L. M. Kistler, T. Mukai, and A. Nishida (2001), Compressional Pc5 type pulsations in the morningside plasma sheet, Ann. Geophys., 19, 311.

Viall, N. M., L. Kepko, and H. E. Spence (2009), Relative occurrence rates and connection of discrete 790 frequency oscillations in the solar wind density and dayside magnetosphere, J. Geophys. Res., 114, A01201, doi:10.1029/2008JA013334.

Walach, M. -T. ., and S. E. Milan (2015), Are steady magnetospheric convection events prolonged substorms?. J. Geophys. Res. Space Physics, 120, 1751–1758. doi: 10.1002/2014JA020631.

Watt, C. E. J., A. W. Degeling, R. Rankin, K. R. Murphy, I. J. Rae, and H. J. Singer (2011), Ultralow-795 frequency modulation of whistler-mode wave growth, J. Geophys. Res., 116, A10209, doi:10.1029/2011JA016730.

Woodger, L. A., A. J. Halford, R. M. Millan, M. P. McCarthy, D. M. Smith, G. S. Bowers, J. G. Sample, B. R. Anderson, and X. Liang (2015), A Summary of the BARREL Campaigns: Technique for studying electron precipitation, Journal of Geophysical Research, 120(6) doi:10.1002/2014JA020874.

800 Xu, B.-L., J. C. Samson, W. W. Liu, F. Creutzberg, and T. J. Hughes (1993), Observations of optical aurora modulated by resonant Alfv6n waves, J. Geophys. Res., 98, 11,531.

Yeoman, T. K. and D. M. Wright (2001), ULF waves with drift resonance and drift-bounce resonance energy sources as observed in artificially-induced HF radar backscatter, Ann. Geophys., 19, 159-170.

Zhang, J., et al. (2016), EMIC waves and associated relativistic electron precipitation on 25–26 805 January 2013, J. Geophys. Res. Space Physics, 121, 11,086–11,100, doi:10.1002/2016JA022918.

Zhou, X.-Y., K. Fukui, H. C. Carlson, J. I. Moen, and R. J. Strangeway (2009), Shock aurora: Ground-based imager observations, J. Geophys. Res., 114, A12216, doi:10.1029/2009JA014186.

Zhu, X., and M. G. Kivelson (1994), Compressional ULF waves in the outer magnetosphere:, 2. A case study of Pc 5 type wave activity, J. Geophys. Res., 99(A1), 241–252, doi:10.1029/93JA02106.

810   Ziauddin, S. (1960), Simultaneous observations of pulsations in the geomagnetic field and in ionospheric absorption, Can. J. Phys., 38(12), 1714–1715.
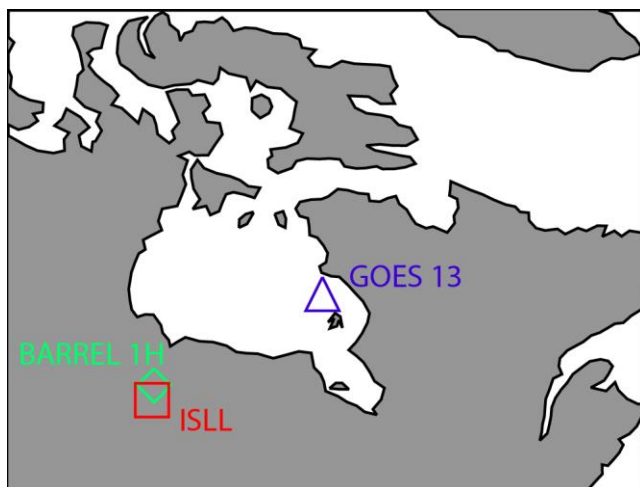
Figures

Figure 1. An overview of the relevant instrumentation for a case study on 26th January 2013 from 1930-2130 UT, projected into the ionosphere using the Tsyganenko 96 magnetic field model (Tsyganenko, 1995). During this event, the BARREL 1H balloon, situated in the southern hemisphere, was immediately conjugate to the ISLL NORSTAR riometer, at dipole L of ~5.2, with the geostationary GOES-13 satellite around 1 hour of local time to the East.
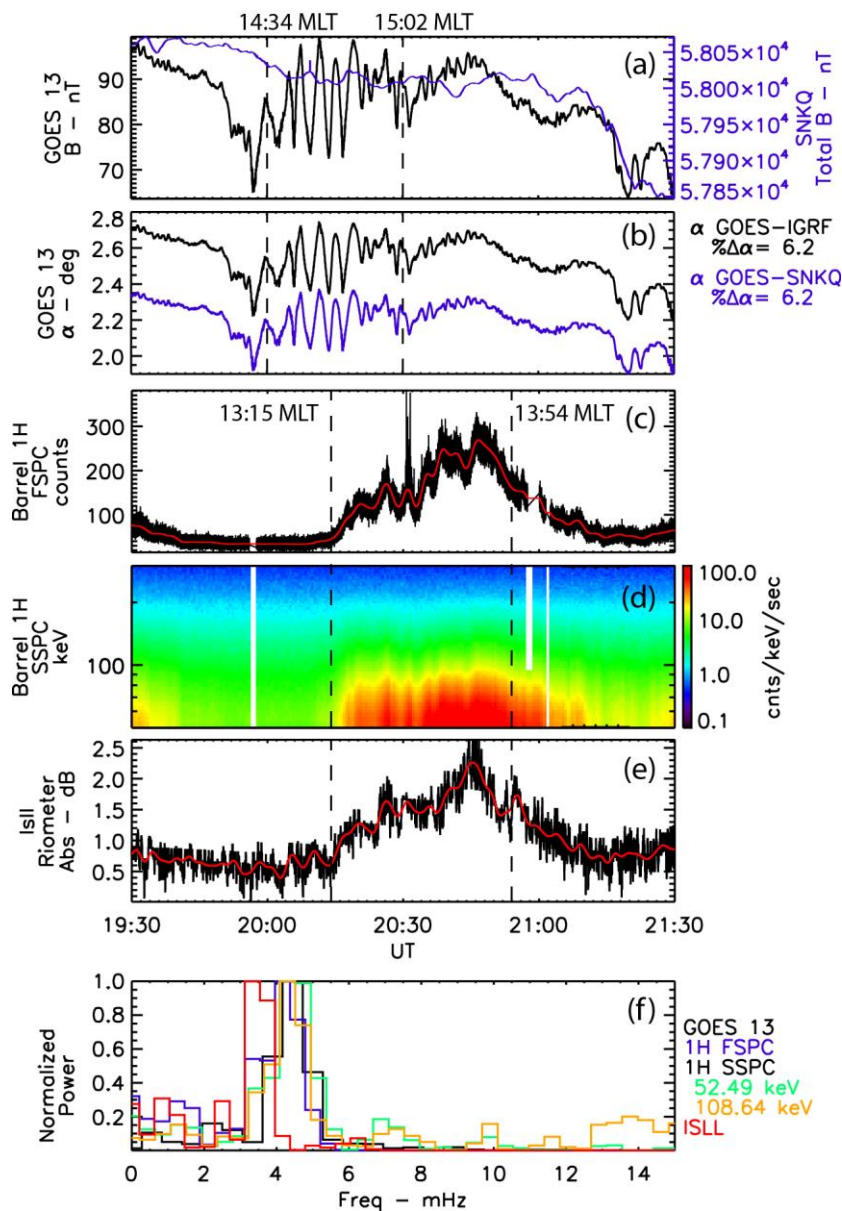
Figure 2. Measurements from the case study on 26th January 2013 from 1930-2130 UT. (a) GOES-13 and conjugate ground magnetometer magnetic field magnitudes, (b) modulation of the loss cone using measured and modeled ionospheric magnetic fields (to be discussed later), (c) channel 1 from the BARREL fast spectra of <180 keV X-rays, (d) BARREL 1H slow spectra from 50-300keV X-rays, (e) riometer absorption from ISLL, and (f) shows the normalized frequency content of each of these datasets calculated within the vertical lines using FFT analysis of the respective time series from GOES-13 (black), BARREL fast- (blue) and slow- (green and yellow) spectra and the ISLL riometer (red).
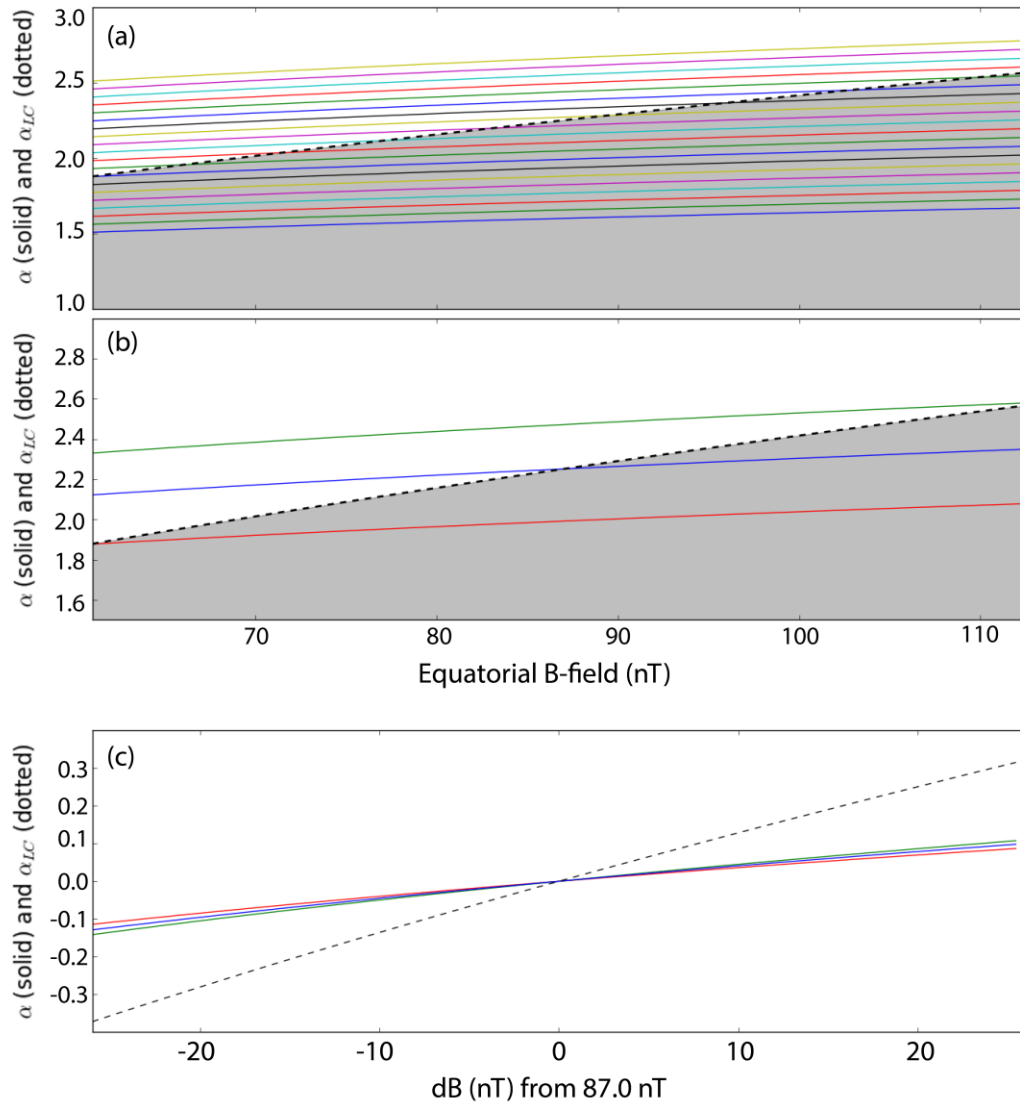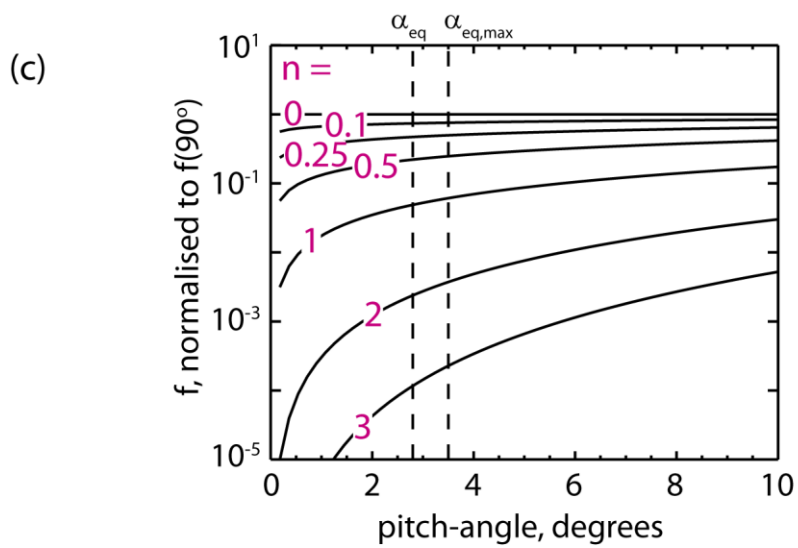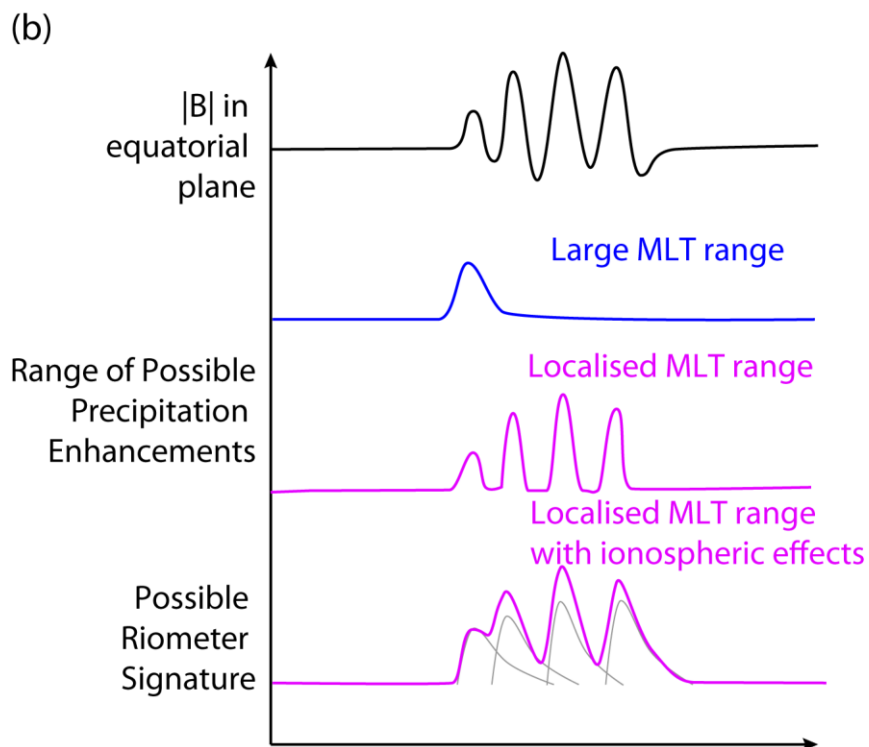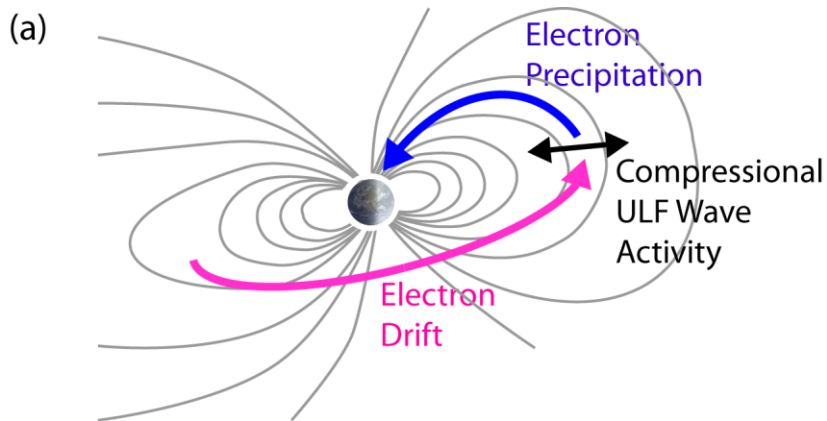
825

830

Figure 3. Demonstration of how equatorial pitch angles $\alpha_{eq,G}$ vary in a slowly varying magnetic field under the assumption of conservation of the first and second adiabatic invariants but not the third invariant (after Halford et al., 2015). Figure 3(a) shows the range of small particle pitch-angles (colored lines) and their variation according to equation (1). The expected change in the BLC due to a ULF wave with an amplitude of 13 nT is denoted as a dashed line, with pitch

835 angles less than that and hence within the BLC shaded in grey. Coloured lines denote sample pitch angles and their variation due due to conservation of the first and second. Figure 3(b) shows important pitch-angles for the case study shown in Figure 2. If only the average magnetic field is considered, the pitch-angle where the blue (upper) solid line crosses the dashed line would indicate the largest particle pitch-angle to be lost into the BLC. Where the green (lower) solid line crosses the dashed line indicates the largest pitch-angle that would be lost under the action of the ULF wave. Figure 3(c)

840 shows the fractional change in α(eq,f) (solid lines) and α_G (dashed line) to demonstrate that the changes in the BLC are indeed much larger than the changes in the particle equatorial pitch angles and that, for larger and larger ULF wave fields, this effect becomes more and more pronounced.

(a) Electron Precipitation · Compressional ULF Wave Activity · Electron Drift

(b) |B| in equatorial plane · Large MLT range · Range of Possible Precipitation Enhancements · Localised MLT range · Localised MLT range with ionospheric effects · Possible Riometer Signature

(c) α_{eq} · $\alpha_{eq,max}$ · $n = 0$, 0.1, 0.25, 0.5, 1, 2, 3 · f, normalised to $f(90°)$ · pitch-angle, degrees

845　　*Figure 4. (a) Schematic representation of the noon-midnight meridian of Earth's magnetosphere indicating the direction of electron drift, a possible region of compressional ULF wave activity on the dayside, the proposed generation mechanism for localized compressional waves and the resulting electron precipitation. (b) Theoretical variations of phase space density at a particular energy as a function of equatorial pitch-angle. Following Gu et al., (2011), we use $f = f_0 \sin^n \alpha_G$, where possible values of n are indicated in the Figure. The median and maximum bounce loss cone angles for the event shown in Figure 1*

850　　*are indicated by vertical dashed lines. (c) Predicted enhancements in precipitation as a function of time in response to a perturbation in |B| in the equatorial plane due to a compressional ULF wave. Different scenarios are demonstrated – one where global ULF compressional oscillations lead to an enhanced loss-cone at all local times, and one where either localisation of the ULF waves, or an external source of drifting electrons, leads to modulation in the precipitation. The bottom trace indicates the predicted riometer signature given the likely ionospheric response to energetic particle*

855　　*precipitation.*
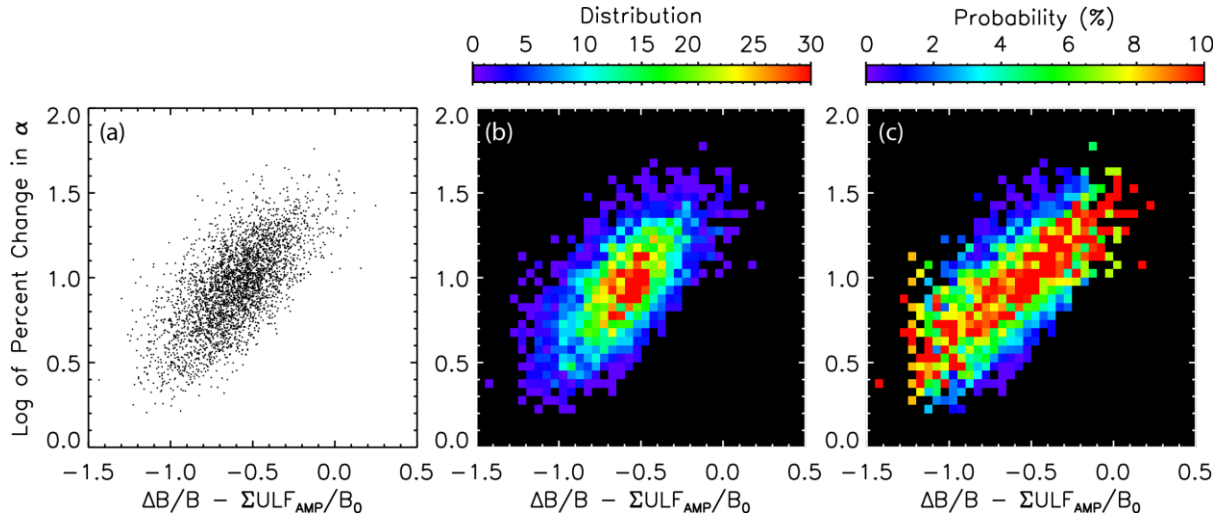
Figure 5. Statistical analysis of GOES West compressional ULF wave events from 1995-2008. (a) shows a scatter plot of the percent change in α_G against dB/B_0 on a logarithmic scale. (b) shows a two dimensional histogram of the events in (a),

860　　*where colour represents the number of events in 0.1x0.1 bins, in log space, (c) shows the probability distribution function (PDF) of observing a given percent change for a given dB/B_0, also in 0.1x0.1 bins on a log scale, such that each column adds up to 100%.*